Climate variability along the margin of the southern African monsoon region at the end of the African Humid

Brian Chase, Arnoud Boom, Andrew Carr, Paula Reimer

Climate variability along the margin of the southern African monsoon region at the end of the African Humid Period

The author does not recommend the distribution of this version of this article.

The article is freely available upon request.

To receive a copy, please send a request to Brian Chase at: brian.chase@umontpellier.fr

Brian M. Chase*[,a,b], Arnoud Boom[c], Andrew S. Carr[c], Paula J. Reimer[d]

[a]*Institut des Sciences de l'Evolution-Montpellier (ISEM), University of Montpellier, Centre National de la Recherche Scientifique (CNRS), EPHE, IRD, Montpellier, France;*

[b]*Department of Environmental and Geographical Science, University of Cape Town, South Lane, Upper Campus, 7701 Rondebosch, South Africa;*

[c]*School of Geography, Geology and the Environment, University of Leicester, Leicester, LE1 7RH, UK;*

[d]*School of Natural and Built Environment, Geography, Archaeology and Palaeoecology, Queen's University Belfast, Belfast, BT7 1NN, Northern Ireland, UK*

***Correspondence and requests should be addressed to:** Brian.Chase@umontpellier.fr, +33 (0)6 01 06 64 04*

Abstract

Evidence for climate variability in the Southern African monsoon region (SAMR) is limited by a spatially and temporally discontinuous palaeoclimatic dataset. We describe a 6680 year long, largely sub-decadal resolution $\delta^{15}N$ record from a rock hyrax midden from southeastern Africa. The results provide a detailed reconstruction of regional hydroclimates since the beginning of the mid-Holocene. A long-term – albeit subtle – increase in humidity consistent with precessional forcing is observed, but the record is dominated by a strong ~1750-yr cycle, a signal that is shared with other SAMR records. Considered in their regional context, these data suggest that changes coincident with the termination of the African Humid Period at ~5500 cal BP do not express the abrupt transition observed in some records from the northern African tropics. Rather they indicate gradual changes, as observed at peri-equatorial sites. Notably, however, eastern and western subregions of the SAMR experience a rapid phase shift beginning ~5500 cal BP, with initially in-phase hydroclimate anomalies transitioning to the establishment of a strong east-west dipole. This likely reflects a coeval strengthening of the Southeast Atlantic trade winds and decreased atmospheric pressure in southeast Africa, factors associated with increasing (decreasing) austral (boreal) summer insolation. The results highlight the distinct nature of southern African responses across this key period of African climate history.

Keywords

Holocene; African Humid Period; southern Africa monsoon region; rock hyrax middens; stable isotopes

Highlights

- High resolution 6680-yr hydroclimate record from southern Africa monsoon region.
- Regionally coherent pattern of mid- to late Holocene climate change.
- Rapid phase change at ~5500 cal BP establishes a strong E-W dipole.
- Dipole linked to high and low latitude forcing driving land-sea pressure gradients.

1 Introduction

Discussions of Holocene climate change in Africa are dominated by consideration of the influence of direct insolation forcing and the processes by which this translates to regional precipitation variability. Most broadly, predictions (Braconnot et al., 2012; Kutzbach, 1981; Kutzbach and Street-Perrott, 1985) and to an extent observations (deMenocal et al., 2000; Garcin et al., 2018; Holmgren et al., 2003; Schefuß et al., 2011; Shanahan et al., 2015; Tierney et al., 2008; Trauth et al., 2018; Weldeab et al., 2007; cf. Chase et al., 2009; Chase et al., 2010) suggest a positive relationship between tropical precipitation and summer insolation. Syntheses of data confirm this, identifying a phase of increased humidity in the northern, central and eastern African tropics (COHMAP, 1988; Gasse, 2000; Shanahan et al., 2015) referred to as the African Humid Period (deMenocal et al., 2000), consistent with increased boreal summer insolation between ~15-5 ka.

However, both data and modelling experiments (e.g. Claussen and Gayler, 1997; Claussen et al., 1999; Dallmeyer et al., 2020; Joussaume et al., 1999) indicate that the African Humid Period is often not defined by a simple linear relationship with insolation. Rather, the spatio-temporal structure is proposed to have been modified by a variety of factors internal to the Earth system, including vegetation-feedbacks and regional circulation dynamics. The influence of glacial boundary conditions is evident in the nature of the onset and early portions of the African Humid Period, often being marked by signals consistent with the ice-forced events (e.g. the Younger Dryas; deMenocal et al., 2000; Menviel et al., 2021; Tierney et al., 2008; Trauth et al., 2018; Weldeab et al., 2007). The termination of the African Humid Period is evidenced as having more diversity in its expression (perhaps somewhat indicative of a greater number of records from the

mid- to late Holocene). Some records indicating gradual transitions to drier conditions (e.g. Kröpelin et al., 2008; Trauth et al., 2018) - in some cases similar in timing to reductions in summer insolation (Garcin et al., 2018; Weldeab et al., 2007) - while other records imply very rapid aridification, resulting from non-linear feedbacks (deMenocal et al., 2000; Tierney et al., 2008). The timing of the onset of the African Humid Period termination is also variable, beginning as early ~7 ka in some records (Garcin et al., 2018), and, arguably, as late as ~3 ka in others (Schefuß et al., 2005; Shanahan et al., 2015; cf. Collins et al., 2017), depending on how the structure of the termination is defined.

Absent from most considerations of the nature and drivers of the African Humid Period is how the South African monsoon region (SAMR; sensu Wang and Ding, 2008; Figure 1) responded to the forcing mechanisms and changes in circulation systems drove such widespread humidity in northern, central and eastern Africa. In southern Africa, the potential to evaluate even low frequency orbital scale patterns of hydroclimate anomalies has been hindered by a lack of continuous, well-resolved Holocene records from the region's semi- to hyper-arid environments, where lake and wetland deposits are rare and landscape data (lake shorelines and dunes) are often of insufficient continuity and temporal resolution (see reviews of Burrough and Thomas, 2013; Chase and Meadows, 2007; Scott et al., 2022).

Along the southwestern distal margin of the SAMR (Figure 1), a greater diversity of archives and proxies have been analysed, including those from Kathu Pan (Beaumont et al., 1984; Scott, 1999; Sobol et al., 2022), Equus Cave (Scott, 1987), Wonderwerk Cave (Brook et al., 2010), Baden-Baden (van Aardt et al., 2016), Florisbad (Scott and Nyakale, 2002), Deelpan (Scott, 1988)

and Blydefontein (Scott et al., 2005). While these archives are characterised by at least some phases of continuous deposition, they often include significant hiatuses and the proxies themselves generally exhibit high noise to signal ratios, rendering it difficult to identify coherent patterns of environmental variability, even when comparing adjacent sites (e.g. Equus and Wonderwerk caves; Scott et al., 2012; Scott et al., 2022). Some success has been achieved in efforts to extract reliable regional signals for specific climatic parameters (e.g. mean annual temperature, wet-season precipitation) using a probability density function based method (Chevalier et al., 2014) to define climate-pollen type relationships (Chevalier and Chase, 2015), but the nature of the underlying proxy data, and quality of the archives themselves remain significant constraints.

Notwithstanding, some continuous terrestrial records from the SAMR have been recovered notably from Lake Ngami (Cordova et al., 2017), Wonderkrater (Scott, 1982) and Tswaing Crater (Kristen et al., 2010; Metwally et al., 2014; Partridge et al., 1997; Scott, 1999), cave sites such as Cold Air Cave (Holmgren et al., 2003; Lee-Thorp et al., 2001), baobabs (Woodborne et al., 2015) and rock hyrax middens from the Namib Desert and the eastern Karoo (Chase et al., 2010; Chase et al., 2009; Chase et al., 2019b; Scott et al., 2005)(Figure 1). The resolution of these records ranges from multi-centennial to multi-millennial for the lake and wetland sites to sub- to multi-decadal for the speleothem and most rock hyrax midden records. Such records potentially enable an evaluation of orbital-scale trends and in some cases scrutiny of significantly more detailed patterns of environmental variability. Where higher resolution records have been obtained, such as the speleothem $\delta^{13}C$ record from Cold Air Cave (Holmgren et al., 2003; Lee-Thorp et al., 2001), it is apparent that the Holocene was characterised by high

frequency, high amplitude climate variability, illustrating the difficulties of extracting meaningful information from low resolution sequences and records.

This extends to the assessment of even long-term trends, including the predicted influence of precessional forcing. Increasing austral summer insolation is predicted to result in progressively more humid conditions from the early to late Holocene (Chase, 2021; COHMAP, 1988; Partridge et al., 1997), and indeed in the northeastern SAMR, records do indicate such a trend (Chevalier and Chase, 2015; Holmgren et al., 2003; Partridge et al., 1997; Schefuß et al., 2011). However, evidence from the distal margin of the SAMR is more ambiguous (Chevalier and Chase, 2015; Scott et al., 2022), and, in the case of the Namibian records, actually indicative of progressive aridification across the Holocene, similar to trends observed in the Northern Hemisphere (Chase et al., 2010; Chase et al., 2009; Chase et al., 2019b).

To address these issues and establish a more cohesive basis for the analysis of regional palaeoclimate variability, we present a high-resolution stable nitrogen isotope record derived from a rock hyrax midden from the southeastern margin of the SAMR. Sampled quasi-continuously with an average sampling interval of 8 years across the last 6680 years, this record is sufficiently detailed to reliably characterise past climate change across what is recognised to be the termination of the African Humid Period – between 6000-2500 cal BP (according to the equatorial and Northern Hemisphere synthesis of Shanahan et al. (2015)). These new data are presented in a regional context that is used to elucidate the nature of climate variability in the SAMR across this key period.

1.1 Regional climate context

In palaeoenvironmental studies, the climate of southern Africa is commonly characterised using a tripartite system of winter, summer and aseasonal rainfall zones (Chase and Meadows, 2007; Deacon and Lancaster, 1988; van Zinderen Bakker, 1976)(Figure 1). This zonation reflects the diverse influences of the large-scale global circulation systems at subtropical latitudes. Rainfall in the southwestern Cape is primarily received during the winter months (the winter rainfall zone; WRZ) when the extratropical southern westerlies are in their northernmost position and associated midlatitude frontal systems exert a more significant influence (Reason et al., 2002). In contrast, much of the subcontinent experiences a summer rainfall regime (the summer rainfall zone; SRZ) determined by tropical convection potential and the transport of moisture from the southwest Indian Ocean and Agulhas Current region in the east (Crétat et al., 2012; Rouault et al., 2002; Tyson et al., 2002) and the tropical Atlantic in the west (Crétat et al., 2019; Rouault et al., 2003). Tropical and extratropical systems also commonly combine to produce significant summer rainfall in southern Africa, as cloud bands referred to as tropical-temperate troughs (TTTs) form when tropical moisture transport and convection combine with extratropical frontal systems (Hart et al., 2010; Todd and Washington, 1999).

The southern African SRZ is broadly coincident with the SAMR, extending further into drier regions (Figure 1), but being determined by the same atmospheric and oceanic circulation systems. While monsoon regions have traditionally been defined according to a seasonal reversals of low-level winds (Ramage, 1971), recent, more inclusive definitions are based on precipitation seasonality and amount (Wang and Ding, 2008; Yim et al., 2014). Using a monsoon precipitation index (MPI) - the local annual range of precipitation (five-month summer minus five-

month winter; NDJFM minus MJJAS in southern Africa) normalized by the annual mean precipitation - a monsoon region is identified as an area where the MPI is greater than 50% and mean annual precipitation is >300 mm (Wang and Ding, 2008).

1.2 Site Description

This study details results from a rock hyrax midden collected from a cliff (28.912°S, 27.435°E) in the sandstone tablelands associated with the Korannaberg and Ribboksberg massifs 45 km north of Maseru and 13 km to the west of Clocolan (Figure 1, 2). Part of the foothills northwest of the Drakensberg Mountains and Lesotho, the site is situated at ~1700 m.a.s.l., and is characterised by mesic highveld vegetation of the Grassland Biome (Eastern Free State Sandy and Clay Grasslands and Basotho Montane Shrubland (Mucina et al., 2006)). Much of the landscape is dominated by grass cover, primarily comprising C_4 varieties (e.g. *Eragrostis*, *Themeda*, *Aristida*) with rarer C_3 genera (e.g. *Erharta*, *Agrostis*, *Helictotrichon*) (Mucina et al., 2006; SANBI, 2003). The talus slopes below the mesas that mark the landscape – including the slope below the Marakabi midden site - support dense shrub (C_3) vegetation dominated by species of *Buddleja*, *Searsia*, *Olea*, *Euclea* and *Diospyros*. The region receives ~720 mm of rainfall per annum, the vast majority of which falls in the summer months (Figure 1). This represents one of the most humid environments in southern Africa for which it has been possible to obtain a continuous rock hyrax midden record (see Chase et al., 2012), and reflects the potential to greatly expand the climatic range within which this specific archive and its associated proxies can be employed.

2 Material and methods

The rock hyrax midden (a stratified accumulation of urine and faecal material) was selected for its thickness and high hyraceum (crystallised urine) content. Proxies obtained from hyraceum are considered to represent environmental conditions more clearly than samples containing high proportions of faecal pellets, which may potentially include a degree of dietary bias (Chase et al., 2012). A representative 85 cm thick section of the midden (referred to as Marakabi-1) (Figure 2) was cut perpendicular to the stratigraphy using an angle grinder and transported back to the laboratory for analysis. During transport, the midden fractured into three sections, subsequently labelled 1a, 1b and 1c. In the lab, the sections were cleaned using progressively finer grades of sandpaper prior to sampling.

2.1 Chronology

Radiocarbon age determinations for the Marakabi-1 midden (n=21) were processed at the ^{14}CHRONO Centre, Queen's University Belfast using accelerator mass spectrometry (AMS) (Table 1; Figure 3). Samples were pre-treated with 2% HCl for one hour at room temperature to remove carbonates and dried at 60°C. They were then weighed into quartz tubes with an excess of CuO, sealed under vacuum and combusted to CO_2. The CO_2 was converted to graphite on an iron catalyst using the zinc reduction method (Slota et al., 1987). The radiocarbon ages were corrected for isotope fractionation using the AMS measured $\delta^{13}C$. The ages were calibrated using the SHCal20 calibration data (Hogg et al., 2020) except for the top sample of section 1A with a 'modern' age where the SHZ1_2 compilation (Hua et al., 2021) was used with 1-year smoothing. The rbacon v.2.5.6 software package (Blaauw and Christen, 2011; Blaauw et al., 2020) was used

to generate the age-depth models for each midden section (Figure 3). Considering the nature of the age model, the midden was considered to still be actively accumulating, and a surface age estimate of the year of collection (2013) was included in the construction of the age model.

2.2 Stable nitrogen isotopes

The stable nitrogen isotope composition of 835 hyraceum samples (approx. 2 mg) were measured at the School of Geography, Geology and the Environment, University of Leicester. Samples were obtained from two offset tracks using a 1 mm drill, creating a quasi-continuous record of overlapping samples. Isotope ratios were measured on a Sercon 20-20 continuous flow isotope ratio mass spectrometer. For the stable isotope analyses, the standard deviation derived from replicate analyses of homogeneous material was better than 0.2‰. Results are expressed relative to atmospheric nitrogen.

3 Results and interpretive basis

3.1 Chronology

Radiocarbon analyses indicate that the Marakabi-1 hyrax midden accumulated during the mid- to late Holocene, spanning the last ~6680 years cal (calibrated) BP. The age-depth models for the three midden sections indicate continuous deposition, although accumulation rates vary in the late Holocene (Table 1; Figure 3). Accumulation rates for the Marakabi-1 midden average ~1 mm/4.7 years for the lower sections, and ~1 mm/11.9 years after ~3000 cal BP. Figure 4 provides information regarding the age uncertainties associated with each stable nitrogen isotope sample, which averages 138±43 years over the whole of the sequence, ranging from averages of 240±69 years to 118±15 years for low and high accumulation rate sections respectively.

3.2 Stable nitrogen and their interpretation

The $\delta^{15}N$ values from the Marakabi-1 midden vary from -1.1 to 9.3‰ (Figure 4). Analyses of modern soil samples taken from the overhang and immediately surrounding slopes (6.7±2‰ n=7) as well as modern faecal pellets from around this site (8±2‰; Carr et al., 2016) compare well with the most recent hyraceum values. Variations in midden $\delta^{15}N$ are interpreted to reflect changes in water availability (see more extensive discussion in Chase et al., 2012). This is considered to generally be a function of a more open nitrogen cycle in arid regions. Fractionating pathways in the soil (nitrification, denitrification, etc.) mean that nitrogen lost through transformation and the release of gaseous products is depleted in ^{15}N, and the remaining nitrogen in the soil is enriched. In more humid regions, N is cycled between live and dead organic pools, while in drier regions more N flows to mineral pools where it is subject to gaseous loss of lighter ^{14}N (Austin and Vitousek, 1998). The $\delta^{15}N$ value of soils is thus higher with increasing aridity (Handley et al., 1999; Murphy and Bowman, 2009). The environmental processes relating to this recycling or loss of ^{15}N are not necessarily tied specifically to rainfall amount, but are more accurately considered to relate to water availability (Murphy and Bowman, 2006), which is in part modulated by changes in temperature and potential evapotranspiration (Chevalier and Chase, 2016). The relationship recognised between aridity and soil ^{15}N is transmitted to, and replicated in, plant and animal tissues, including herbivore faecal matter (e.g. Aranibar et al., 2008; Carr et al., 2016; Craine et al., 2009; Hartman, 2011; Hartman and Danin, 2010; Murphy and Bowman, 2006; Newsome et al., 2011; Swap et al., 2004). Studies of ^{15}N in hyrax middens from a wide range of environments indicate consistently strong correlations between midden ^{15}N and independent climate proxy records, supporting the conclusion that environmental moisture

availability is a major driver of midden ^{15}N records (Carr et al., 2016; Chase et al., 2015a; Chase et al., 2017; Chase et al., 2009; Chase et al., 2019b).

4 Discussion

The Marakabi-1 hyraceum $\delta^{15}N$ record – interpreted primarily as a proxy for water availability – exhibits a slight long-term decrease (indicating increased humidity) across the mid- to late Holocene, but is characterised by a marked ~1750-yr cycle (Figure 4). To our knowledge, the latter has not been reported previously. Comparison with other highly resolved records from the SAMR, such as the stable isotope records from the Cold Air Cave speleothems (Holmgren et al., 2003) and further afield at Lake Ngami (Cordova et al., 2017), indicate similar patterns of orbital and suborbital climate variability (Figure 5). These records suggest a long term increase in humidity in the eastern and central SAMR, consistent with the predicted influence of precessional forcing in the low southern latitudes (COHMAP, 1988). The relatively minor increase in humidity seen in the Marakabi-1 record compared to sites closer to the core of the SAMR (Chevalier and Chase, 2015; Holmgren et al., 2003), suggests a progressive decline in the significance of this mechanism as one approaches the distal margin of the SAMR domain. During the last millennium, conditions in the central and eastern SAMR indicate a marked shift towards drier conditions, consistent with the observed ~1750-yr cycle. Current conditions at Marakabi are shown to be some of the driest (highest $\delta^{15}N$ values) of the last 6700 years.

In contrast, rock hyrax midden $\delta^{15}N$ records from South Africa's winter rainfall zone, from Katbakkies Pass (Chase et al., 2015b) and – to a lesser degree – Pakhuis Pass (Chase et al., 2019a), indicate a general antiphase relationship in the pattern of humid and arid episodes (Figure 5).

This is consistent with conceptual models suggesting an inverse relationship exists between temperate and tropical systems in South Africa, with periods of increased humidity in the winter rainfall zone a result of equatorward displacements of the westerly storm track, resulting in a diminished influence of tropical systems and relative aridity in the summer rainfall zone (Chase et al., 2017; Cockcroft et al., 1987; van Zinderen Bakker, 1976).

The Marakabi-1 data provide valuable evidence for environmental change from southeastern Africa (Figure 1) and an opportunity to evaluate spatio-temporal aspects of climate change along the distal margin of the SAMR. Employing the Marakabi-1 data and a high-resolution southwest African correlate from Spitzkoppe (Chase et al., 2009; Chase et al., 2019b), just beyond the modern SAMR margin in the Namib Desert (Figure 1), it is possible to define a broader picture of climate dynamics across the mid- to late Holocene. Despite the distance between the sites (1450 km), a remarkably strong relationship is observed between the Marakabi-1 and Spitzkoppe 2012-1 (Chase et al., 2019b) $\delta^{15}N$ records (Figure 6). Particularly interesting is the manner in which this relationship evolves across the mid-Holocene. Prior to ~5500 cal BP, a strong positive correlation is evident between the Marakabi and Spitzkoppe $\delta^{15}N$ records at the dominant ~1750-yr period (Figure 6). This suggests that patterns of climate variability were similar between eastern and western sub-regions of the SAMR, with, perhaps, the southwestern limit of SAMR extending further to the south. At ~5500 cal BP, this relationship begins to weaken, and by ~3900 cal BP a strong negative relationship is established at the same frequency, indicating that while the underlying mechanism determining climate variability is the same for both the eastern and western SAMR, the response is inverted, and the late Holocene is characterised by a strong E-W dipole.

It is notable that the ~5500 - 3900 cal BP period corresponds with the final phase of the African Humid Period, as evidenced by records from the Northwest African subtropics (deMenocal et al., 2000; Shanahan et al., 2015; Tierney et al., 2017). In the context of debates regarding the nature of the African Humid Period Termination – and whether it was abrupt (Claussen et al., 1999; deMenocal et al., 2000), gradual (Kröpelin et al., 2008), or spatio-temporally complex (Shanahan et al., 2015) – the data from Spitzkoppe (Chase et al., 2009; Chase et al., 2019b) and Marakabi do not indicate an abrupt termination, but rather a gradual trend towards drier and wetter conditions respectively. What is remarkable, however, is the rapid nature in which the E-W dipole is established (Figure 6), and its concurrence with the establishment of arid conditions in the northern African tropics that mark the termination of the African Humid Period (as inferred from the ODP 658C dust record of deMenocal et al. (2000) (Figure 6)).

We associate the establishment of this E-W dipole with changes in regional atmospheric pressure fields and the extent of the African tropical rainbelt. Our data suggest that during the mid-Holocene the tropical rain belt influenced both eastern and western portions of the subcontinent in a similar fashion, likely through a dominance of easterly flow. As Northern Hemisphere summer insolation decreased from the mid- to late Holocene, the South Atlantic Anticyclone and Benguela upwelling system strengthened (Farmer et al., 2005; Kim et al., 2003) due to increased hemispheric temperature gradients (Figure 7). This may have resulted in an increase in low-level flow from the Atlantic Ocean, creating drier conditions along the western continental margin, as evidenced by data from sites throughout the Namib Desert and adjacent interior (Chase et al., 2010; Chase et al., 2009; Chase et al., 2019b; Scott et al., 1991). In a coeval

inverse response to the same changes in orbital parameters, increasing austral summer insolation over southern Africa reduced atmospheric pressure and favoured convection and the incursion of tropical moisture in southeastern Africa with more humid conditions being observed at Marakabi and sites such as Cold Air Cave (Holmgren et al., 2003) (Figure 7) (Chase et al., 2019b). The strength of the anti-phase relationship between eastern and western regions may have been reinforced through the recurvature of the Southeast Atlantic trade winds across Angola and Zambia as low-level westerlies, bringing moist tropical air to the east even as they inhibited convection and the incursion of moisture bearing systems along the southwest African margin (Figure 7).

5 Conclusions

Data from the Marakabi-1 rock hyrax midden has provided an highly resolved record regarding changes in southeastern African hydroclimate over the last 6680 years. A progressive increase in humidity across the Holocene – as predicted in response to precessional forcing - is apparent in central and eastern SAMR records, but manifests only weakly at Marakabi-1, suggesting a diminished influence of this mechanism at the southern distal margin of the monsoon region. Sites from the southwestern margin of the SAMR indicate, in contrast, a progressive aridification across the Holocene. In both eastern and western subregions, a strong ~1750-yr cyclicity is apparent in the proxy record. Further work is required to establish the origin of this cycle, but its distribution suggests a tropical mechanism. The unique responses between the eastern and western subregions is further highlighted by a marked phase shift in the response to ~1750-yr cycle. Prior to ~5500 cal BP, the eastern and western subregions indicate in-phase hydroclimatic

variability, suggesting a dominant influence of tropical easterly flow in both regions. However, beginning at ~5500 cal BP – coincident with the termination of the African Humid Period – an anti-phase relationship is established, creating a east-west dipole across southern Africa. We associate this with increasing (decreasing) austral (boreal) summer insolation, which drove changes in land-sea pressure gradients that resulted in a strengthening of the Southeast Atlantic trade winds and their recurvature across Angola and Zambia, at once supressing precipitation along the southwest African margin while enhancing the transport of moist tropical air to southeast Africa. Thus, generally synchronous trends of progressive aridification are observed between southwestern Africa and regions of northern, central and eastern Africa with the termination of the African Humid Period, likely as a result of an equatorward contraction of the African rainbelt in these sectors. In contrast, southeastern African records indicate progressively wetter conditions across the mid- to late Holocene, with lower pressure over the subcontinent and increased northerly and northwesterly flow from the tropics resulting in an asymmetric response both between the hemispheres and between western and eastern subregions of southern Africa.

6 Acknowledgements

The research leading to these results has received funding from the European Research Council under the European Union's Seventh Framework Programme (FP7/2007-2013), ERC Starting Grant “HYRAX”, grant agreement no. 258657. We also thank two anonymous reviewers for the constructive comments.

7 References

Aranibar, J.N., Anderson, I.C., Epstein, H.E., Feral, C.J.W., Swap, R.J., Ramontsho, J., Macko, S.A., 2008. Nitrogen isotope composition of soils, C_3 and C_4 plants along land use gradients in southern Africa. Journal of Arid Environments 72, 326-337.

Austin, A.T., Vitousek, P.M., 1998. Nutrient dynamics on a precipitation gradient in Hawai'i. Oecologia 113, 519-529.

Beaumont, P.B., Van Zinderen Bakker Sr, E.M., Vogel, J.C., 1984. Environmental changes since 32 000 BP at Kathu Pan, northern Cape., in: J.C., V. (Ed.), Late Cainozoic palaeoclimates of the Southern Hemisphere. Balkema, pp. 329-338.

Blaauw, M., Christen, J.A., 2011. Flexible paleoclimate age-depth models using an autoregressive gamma process. Bayesian Analysis 6, 457-474.

Blaauw, M., Christen, J.A., A., M., L., A., 2020. rbacon: Age-Depth Modelling using Bayesian Statistics. R package version 2.5.6.

Braconnot, P., Harrison, S.P., Kageyama, M., Bartlein, P.J., Masson-Delmotte, V., Abe-Ouchi, A., Otto-Bliesner, B., Zhao, Y., 2012. Evaluation of climate models using palaeoclimatic data. Nature Clim. Change 2, 417-424.

Brook, G.A., Scott, L., Railsback, L.B., Goddard, E.A., 2010. A 35 ka pollen and isotope record of environmental change along the southern margin of the Kalahari from a stalagmite and animal dung deposits in Wonderwerk Cave, South Africa. Journal of Arid Environments 74, 870-884.

Burrough, S.L., Thomas, D.S.G., 2013. Central southern Africa at the time of the African Humid Period: a new analysis of Holocene palaeoenvironmental and palaeoclimate data. Quaternary Science Reviews 80, 29-46.

Burrough, S.L., Thomas, D.S.G., Shaw, P.A., Bailey, R.M., 2007. Multiphase Quaternary highstands at Lake Ngami, Kalahari, northern Botswana. Palaeogeography, Palaeoclimatology, Palaeoecology 253, 280-299.

Carr, A.S., Chase, B.M., Boom, A., Medina-Sanchez, J., 2016. Stable isotope analyses of rock hyrax faecal pellets, hyraceum and associated vegetation in southern Africa: Implications for dietary ecology and palaeoenvironmental reconstructions. Journal of Arid Environments 134, 33-48.

Chase, B.M., 2021. Orbital forcing in southern Africa: Towards a conceptual model for predicting deep time environmental change from an incomplete proxy record. Quaternary Science Reviews 265, 107050.

Chase, B.M., Boom, A., Carr, A.S., Carré, M., Chevalier, M., Meadows, M.E., Pedro, J.B., Stager, J.C., Reimer, P.J., 2015a. Evolving southwest African response to abrupt deglacial North Atlantic climate change events. Quaternary Science Reviews 121, 132-136.

Chase, B.M., Boom, A., Carr, A.S., Chevalier, M., Quick, L.J., Verboom, G.A., Reimer, P.J., 2019a. Extreme hydroclimate response gradients within the western Cape Floristic region of South Africa since the Last Glacial Maximum. Quaternary Science Reviews 219, 297-307.

Chase, B.M., Chevalier, M., Boom, A., Carr, A.S., 2017. The dynamic relationship between temperate and tropical circulation systems across South Africa since the last glacial maximum. Quaternary Science Reviews 174, 54-62.

Chase, B.M., Lim, S., Chevalier, M., Boom, A., Carr, A.S., Meadows, M.E., Reimer, P.J., 2015b. Influence of tropical easterlies in southern Africa's winter rainfall zone during the Holocene. Quaternary Science Reviews 107, 138-148.

Chase, B.M., Meadows, M.E., 2007. Late Quaternary dynamics of southern Africa's winter rainfall zone. Earth-Science Reviews 84, 103-138.

Chase, B.M., Meadows, M.E., Carr, A.S., Reimer, P.J., 2010. Evidence for progressive Holocene aridification in southern Africa recorded in Namibian hyrax middens: implications for African Monsoon dynamics and the "African Humid Period''. Quaternary Research 74, 36-45.

Chase, B.M., Meadows, M.E., Scott, L., Thomas, D.S.G., Marais, E., Sealy, J., Reimer, P.J., 2009. A record of rapid Holocene climate change preserved in hyrax middens from southwestern Africa. Geology 37, 703-706.
Chase, B.M., Niedermeyer, E.M., Boom, A., Carr, A.S., Chevalier, M., He, F., Meadows, M.E., Ogle, N., Reimer, P.J., 2019b. Orbital controls on Namib Desert hydroclimate over the past 50,000 years. Geology.
Chase, B.M., Scott, L., Meadows, M.E., Gil-Romera, G., Boom, A., Carr, A.S., Reimer, P.J., Truc, L., Valsecchi, V., Quick, L.J., 2012. Rock hyrax middens: a palaeoenvironmental archive for southern African drylands. Quaternary Science Reviews 56, 107-125.
Chevalier, M., Chase, B.M., 2015. Southeast African records reveal a coherent shift from high- to low-latitude forcing mechanisms along the east African margin across last glacial–interglacial transition. Quaternary Science Reviews 125, 117-130.
Chevalier, M., Chase, B.M., 2016. Determining the drivers of long-term aridity variability: a southern African case study. Journal of Quaternary Science 31, 143-151.
Chevalier, M., Cheddadi, R., Chase, B.M., 2014. CREST (Climate REconstruction SofTware): a probability density function (*pdf*)-based quantitative climate reconstruction method. Clim. Past 10, 2081-2098.
Claussen, M., Gayler, V., 1997. The Greening of the Sahara during the mid-Holocene: results of an interactive atmosphere-biome model. Global Ecology and Biogeography Letters 6, 369-377.
Claussen, M., Kubatzki, C., Brovkin, V., Ganopolski, A., Hoelzmann, P., Pachur, H.-J., 1999. Simulation of an abrupt change in Saharan vegetation in the Mid-Holocene. Geophysical Research Letters 26, 2037-2040.
Cockcroft, M.J., Wilkinson, M.J., Tyson, P.D., 1987. The application of a present-day climatic model to the late Quaternary in southern Africa. Climatic Change 10, 161-181.
COHMAP, 1988. Climatic changes of the last 18,000 years: observations and model simulations. Science 241, 1043-1052.
Collins, J.A., Prange, M., Caley, T., Gimeno, L., Beckmann, B., Mulitza, S., Skonieczny, C., Roche, D., Schefuß, E., 2017. Rapid termination of the African Humid Period triggered by northern high-latitude cooling. Nature Communications 8, 1372.
Cooper, G.R.J., Cowan, D.R., 2008. Comparing time series using wavelet-based semblance analysis. Computers & Geosciences 34, 95-102.
Cordova, C.E., Scott, L., Chase, B.M., Chevalier, M., 2017. Late Pleistocene-Holocene vegetation and climate change in the Middle Kalahari, Lake Ngami, Botswana. Quaternary Science Reviews 171, 199-215.
Craine, J.M., Elmore, A.J., Aidar, M.P.M., Bustamante, M., Dawson, T.E., Hobbie, E.A., Kahmen, A., Mack, M.C., McLauchlan, K.K., Michelsen, A., Nardoto, G.B., Pardo, L.H., Peñuelas, J., Reich, P.B., Schuur, E.A.G., Stock, W.D., Templer, P.H., Virginia, R.A., Welker, J.M., Wright, I.J., 2009. Global patterns of foliar nitrogen isotopes and their relationships with climate, mycorrhizal fungi, foliar nutrient concentrations, and nitrogen availability. New Phytologist 183, 980-992.
Crétat, J., Pohl, B., Dieppois, B., Berthou, S., Pergaud, J., 2019. The Angola Low: relationship with southern African rainfall and ENSO. Climate Dynamics 52, 1783-1803.
Crétat, J., Richard, Y., Pohl, B., Rouault, M., Reason, C., Fauchereau, N., 2012. Recurrent daily rainfall patterns over South Africa and associated dynamics during the core of the austral summer. International Journal of Climatology 32, 261-273.
Dallmeyer, A., Claussen, M., Lorenz, S.J., Shanahan, T., 2020. The end of the African humid period as seen by a transient comprehensive Earth system model simulation of the last 8000 years. Clim. Past 16, 117-140.
Deacon, J., Lancaster, N., 1988. Late Quaternary palaeoenvironments of southern Africa. Clarendon Press, Oxford.
deMenocal, P., Ortiz, J., Guilderson, T., Adkins, J., Sarnthein, M., Baker, L., Yarusinsky, M., 2000. Abrupt onset and termination of the African Humid Period: rapid climate responses to gradual insolation forcing. Quaternary Science Reviews 19, 347-361.

Farmer, E.C., deMenocal, P.B., Marchitto, T.M., 2005. Holocene and deglacial ocean temperature variability in the Benguela upwelling region: implications for low-latitude atmospheric circulation. Paleoceanography 20, doi:10.1029/2004PA001049.
Fick, S.E., Hijmans, R.J., 2017. WorldClim 2: new 1-km spatial resolution climate surfaces for global land areas. International Journal of Climatology 37, 4302-4315.
Garcin, Y., Deschamps, P., Ménot, G., de Saulieu, G., Schefuß, E., Sebag, D., Dupont, L.M., Oslisly, R., Brademann, B., Mbusnum, K.G., Onana, J.-M., Ako, A.A., Epp, L.S., Tjallingii, R., Strecker, M.R., Brauer, A., Sachse, D., 2018. Early anthropogenic impact on Western Central African rainforests 2,600 y ago. Proceedings of the National Academy of Sciences of the United States of America 115, 3261–3266.
Gasse, F., 2000. Hydrological changes in the African tropics since the Last Glacial Maximum. Quaternary Science Reviews 19, 189-211.
Hammer, Ø., Harper, D.A.T., Ryan, P.D., 2001. PAST: Paleontological Statistics Software Package for Education and Data Analysis. Palaeontologia Electronica 4, 9.
Handley, L.L., Austin, A.T., Stewart, G.R., Robinson, D., Scrimgeour, C.M., Raven, J.A., Heaton, T.H.E., Schmidt, S., 1999. The ^{15}N natural abundance ($d^{15}N$) of ecosystem samples reflects measures of water availability. Functional Plant Biology 26, 185-199.
Hart, N.C.G., Reason, C.J.C., Fauchereau, N., 2010. Tropical–Extratropical Interactions over Southern Africa: Three Cases of Heavy Summer Season Rainfall. Monthly Weather Review 138, 2608-2623.
Hartman, G., 2011. Are elevated $\delta^{15}N$ values in herbivores in hot and arid environments caused by diet or animal physiology? Functional Ecology 25, 122-131.
Hartman, G., Danin, A., 2010. Isotopic values of plants in relation to water availability in the Eastern Mediterranean region. Oecologia 162, 837-852.
He, F., Shakun, J.D., Clark, P.U., Carlson, A.E., Liu, Z., Otto-Bliesner, B.L., Kutzbach, J.E., 2013. Northern Hemisphere forcing of Southern Hemisphere climate during the last deglaciation. Nature 494, 81-85.
Hogg, A.G., Heaton, T.J., Hua, Q., Palmer, J.G., Turney, C.S.M., Southon, J., Bayliss, A., Blackwell, P.G., Boswijk, G., Bronk Ramsey, C., Pearson, C., Petchey, F., Reimer, P., Reimer, R., Wacker, L., 2020. SHCal20 Southern Hemisphere Calibration, 0–55,000 years cal BP. Radiocarbon, 1-20.
Holmgren, K., Lee-Thorp, J.A., Cooper, G.R.J., Lundblad, K., Partridge, T.C., Scott, L., Sithaldeen, R., Talma, A.S., Tyson, P.D., 2003. Persistent millennial-scale climatic variability over the past 25,000 years in Southern Africa. Quaternary Science Reviews 22, 2311-2326.
Hua, Q., Turnbull, J.C., Santos, G.M., Rakowski, A.Z., Ancapichún, S., De Pol-Holz, R., Hammer, S., Lehman, S.J., Levin, I., Miller, J.B., Palmer, J.G., Turney, C.S.M., 2021. Atmospheric radiocarbon for the period 1950–2019. Radiocarbon, 1-23.
Joussaume, S., Taylor, K.E., Braconnot, P., Mitchell, J.F.B., Kutzbach, J.E., Harrison, S.P., Prentice, I.C., Broccoli, A.J., Abe-Ouchi, A., Bartlein, P.J., Bonfils, C., Dong, B., Guiot, J., Herterich, K., Hewitt, C.D., Jolly, D., Kim, J.W., Kislov, A., Kitoh, A., Loutre, M.F., Masson, V., McAvaney, B., McFarlane, N., de Noblet, N., Peltier, W.R., Peterschmitt, J.Y., Pollard, D., Rind, D., Royer, J.F., Schlesinger, M.E., Syktus, J., Thompson, S., Valdes, P., Vettoretti, G., Webb, R.S., Wyputta, U., 1999. Monsoon changes for 6000 years ago: results of 18 simulations from the Paleoclimate Modeling Intercomparison Project (PMIP). Geophysical Research Letters 26, 859-862.
Kim, J.-H., Schneider, R.R., Mulitza, S., Müller, P.J., 2003. Reconstruction of SE trade-wind intensity based on sea-surface temperature gradients in the Southeast Atlantic over the last 25 kyr. Geophysical Research Letters 30, 2144.
Kristen, I., Wilkes, H., Vieth, A., Zink, K.-G., Plessen, B., Thorpe, J., Partridge, T.C., Oberhänsli, H., 2010. Biomarker and stable carbon isotope analyses of sedimentary organic matter from Lake Tswaing: evidence for deglacial wetness and early Holocene drought from South Africa. Journal of Paleolimnology 44, 143-160.

Kröpelin, S., Verschuren, D., Lezine, A.M., Eggermont, H., Cocquyt, C., Francus, P., Cazet, J.P., Fagot, M., Rumes, B., Russell, J.M., Darius, F., Conley, D.J., Schuster, M., von Suchodoletz, H., Engstrom, D.R., 2008. Climate-driven ecosystem succession in the Sahara: the past 6000 years. Science 320, 765-768.
Kutzbach, J.E., 1981. Monsoon climate of the early Holocene: climate experiment with the Earth's orbital parameters for 9000 years ago. Science 214, 59-61.
Kutzbach, J.E., Street-Perrott, F.A., 1985. Milankovitch forcing of fluctuations in the level of tropical lakes from 18 to 0 kyr BP. Nature 317, 130-134.
Lee-Thorp, J.A., Holmgren, K., Lauritzen, S.-E., Linge, H., Moberg, A., Partridge, T.C., Stevenson, C., Tyson, P.D., 2001. Rapid climate shifts in the southern African interior throughout the mid- to late Holocene. Geophysical Research Letters 28, 4507-4510.
Lim, S., Chase, B.M., Chevalier, M., Reimer, P.J., 2016. 50,000 years of vegetation and climate change in the southern Namib Desert, Pella, South Africa. Palaeogeography, Palaeoclimatology, Palaeoecology 451, 197-209.
Liu, Z., Otto-Bliesner, B.L., He, F., Brady, E.C., Tomas, R., Clark, P.U., Carlson, A.E., Lynch-Stieglitz, J., Curry, W., Brook, E., Erickson, D., Jacob, R., Kutzbach, J., Cheng, J., 2009. Transient simulation of last deglaciation with a new mechanism for Bølling-Allerød warming. Science 325, 310-314.
Meadows, M.E., Chase, B.M., Seliane, M., 2010. Holocene palaeoenvironments of the Cederberg and Swartruggens mountains, Western Cape, South Africa: Pollen and stable isotope evidence from hyrax dung middens. Journal of Arid Environments 74, 786-793.
Menviel, L., Govin, A., Avenas, A., Meissner, K.J., Grant, K.M., Tzedakis, P.C., 2021. Drivers of the evolution and amplitude of African Humid Periods. Communications Earth & Environment 2, 237.
Metwally, A.A., Scott, L., Neumann, F.H., Bamford, M.K., Oberhänsli, H., 2014. Holocene palynology and palaeoenvironments in the Savanna Biome at Tswaing Crater, central South Africa. Palaeogeography, Palaeoclimatology, Palaeoecology 402, 125-135.
Mucina, L., Hoare, D.B., Lotter, M.C., du Preez, P.J., Rutherford, M.C., Scott-Shaw, C.R., Bredenkamp, G.J., Powrie, L.W., Scott, L., Camp, K.G.T., Cilliers, S.S., Bezuidenhout, H., Mostert, T.H., Siebert, S.J., Winter, P.J.D., Burrows, J.E., Dobson, L., Ward, R.A., Stalmans, M., Oliver, E.G.H., Siebert, F., Schmidt, E., Kobisi, K., Kose, L., 2006. Grassland Biome, in: Mucina, L., Rutherford, M.C. (Eds.), The Vegetation of South Africa, Lesotho and Swaziland. South African National Biodiversity Institute, Pretoria, pp. 349-436.
Murphy, B.P., Bowman, D.M.J.S., 2006. Kangaroo metabolism does not cause the relationship between bone collagen $d^{15}N$ and water availability. Functional Ecology 20, 1062-1069.
Murphy, B.P., Bowman, D.M.J.S., 2009. The carbon and nitrogen isotope composition of Australian grasses in relation to climate. Functional Ecology 23, 1040-1049.
Newsome, S.D., Miller, G.H., Magee, J.W., Fogel, M.L., 2011. Quaternary record of aridity and mean annual precipitation based on $\delta^{15}N$ in ratite and dromornithid eggshells from Lake Eyre, Australia. Oecologia 167, 1151-1162.
NOAA/OAR/ESRL/PSL, NOAA OI SST V2 High Resolution Dataset, in: NOAA/OAR/ESRL PSL, B., Colorado, USA (Ed.), 2.1 ed.
Partridge, T.C., deMenocal, P.B., Lorentz, S.A., Paiker, M.J., Vogel, J.C., 1997. Orbital forcing of climate over South Africa: a 200,000-year rainfall record from the Pretoria Saltpan. Quaternary Science Reviews 16, 1125-1133.
Ramage, C.S., 1971. Monsoon meteorology. Academic Press, New York.
Reason, C.J.C., Rouault, M., Melice, J.L., Jagadheesha, D., 2002. Interannual winter rainfall variability in SW South Africa and large scale ocean–atmosphere interactions. Meteorology and Atmospheric Physics 80, 19-29.
Rouault, M., Florenchie, P., Fauchereau, N., Reason, C.J.C., 2003. South East tropical Atlantic warm events and southern African rainfall. Geophysical Research Letters 30.

Rouault, M., White, S.A., Reason, C.J.C., Lutjeharms, J.R.E., Jobard, I., 2002. Ocean–Atmosphere Interaction in the Agulhas Current Region and a South African Extreme Weather Event. Weather & Forecasting 17, 655.
SANBI, 2003. PRECIS (National Herbarium Pretoria (PRE) Computerized Information System) database.
Schefuß, E., Kuhlmann, H., Mollenhauer, G., Prange, M., Pätzold, J., 2011. Forcing of wet phases in southeast Africa over the past 17,000 years. Nature 480, 509-512.
Schefuß, E., Schouten, S., Schneider, R.R., 2005. Climatic controls on central African hydrology during the past 20,000 years. Nature 437, 1003-1006.
Scott, L., 1982. A late Quaternary pollen record from the Transvaal bushveld, South Africa. Quaternary Research 17, 339-370.
Scott, L., 1987. Pollen analysis of hyena coprolites and sediments from Equus Cave, Taung, southern Kalahari (South Africa). Quaternary Research 28, 144-156.
Scott, L., 1988. Holocene environmental change at western Orange Free state pans, South Africa, inferred from pollen analysis. Palaeoecology of Africa 19, 109-118.
Scott, L., 1999. Vegetation history and climate in the Savanna biome South Africa since 190,000 ka: a comparison of pollen data from the Tswaing Crater (the Pretoria Saltpan) and Wonderkrater. Quaternary International 57-8, 215-223.
Scott, L., Bousman, C.B., Nyakale, M., 2005. Holocene pollen from swamp, cave and hyrax dung deposits at Blydefontein (Kikvorsberge), Karoo, South Africa. Quaternary International 129, 49-59.
Scott, L., Cooremans, B., de Wet, J.S., Vogel, J.C., 1991. Holocene environmental changes in Namibia inferred from pollen analysis of swamp and lake deposits. Holocene 1, 8-13.
Scott, L., Neumann, F.H., Brook, G.A., Bousman, C.B., Norström, E., Metwally, A.A., 2012. Terrestrial fossil-pollen evidence of climate change during the last 26 thousand years in southern Africa. Quaternary Science Reviews 32, 100-118.
Scott, L., Nyakale, M., 2002. Pollen indications of Holocene palaeoenvironments at Florisbad spring in the central Free State, South Africa. Holocene 12, 497-503.
Scott, L., Sobol, M., Neumann, F.H., Gil Romera, G., Fernández-Jalvo, Y., Bousman, C.B., Horwitz, L.K., van Aardt, A.C., 2022. Late Quaternary palaeoenvironments in the central semi-arid region of South Africa from pollen in cave, pan, spring, stream and dung deposits. Quaternary International 614, 84-97.
Scott, L., Woodborne, S., 2007a. Pollen analysis and dating of Late Quaternary faecal deposits (hyraceum) in the Cederberg, Western Cape, South Africa. Review of Palaeobotany and Palynology 144, 123-134.
Scott, L., Woodborne, S., 2007b. Vegetation history inferred from pollen in Late Quaternary faecal deposits (hyraceum) in the Cape winter-rain region and its bearing on past climates in South Africa. Quaternary Science Reviews 26, 941-953.
Shanahan, T.M., McKay, N.P., Hughen, K.A., Overpeck, J.T., Otto-Bliesner, B., Heil, C.W., King, J., Scholz, C.A., Peck, J., 2015. The time-transgressive termination of the African Humid Period. Nature Geoscience 8, 140-144.
Slota, P.J., Jull, A.J.T., Linick, T.W., Toolin, L.J., 1987. Preparation of small samples for ^{14}C accelerator targets by catalytic reduction of CO. Radiocarbon 29, 303-306.
Sobol, M.K., Chazan, M., Scott, L., Finkelstein, S.A., 2022. Characterizing the Meghalayan Stage in southern Africa: A multiproxy record of paleoenvironmental change at the southern margin of the Kalahari. Quaternary International 614, 98-110.
Sundqvist, H.S., Holmgren, K., Fohlmeister, J., Zhang, Q., Bar-Matthews, M., Spötl, C., Körnich, H., 2013. Evidence of a large cooling between 1690 and 1740 AD in southern Africa. Scientific Reports 3.
Swap, R.J., Aranibar, J.N., Dowty, P.R., Gilhooly, W.P., Macko, S.A., 2004. Natural abundance of ^{13}C and ^{15}N in C_3 and C_4 vegetation of southern Africa: patterns and implications. Global Change Biology 10, 350-358.
Tierney, J.E., Pausata, F.S.R., deMenocal, P.B., 2017. Rainfall regimes of the Green Sahara. Science Advances 3, e1601503.

Tierney, J.E., Russell, J.M., Huang, Y., Sinninghe Damsté, J.S., Hopmans, E.C., Cohen, A.S., 2008. Northern Hemisphere controls on tropical southeast African climate during the past 60,000 years. Science 322, 252-255.
Todd, M., Washington, R., 1999. Circulation anomalies associated with tropical-temperate troughs in southern Africa and the south west Indian Ocean. Climate Dynamics 15, 937-951.
Trauth, M.H., Foerster, V., Junginger, A., Asrat, A., Lamb, H.F., Schaebitz, F., 2018. Abrupt or gradual? Change point analysis of the late Pleistocene–Holocene climate record from Chew Bahir, southern Ethiopia. Quaternary Research, 1-10.
Truc, L., Chevalier, M., Favier, C., Cheddadi, R., Meadows, M.E., Scott, L., Carr, A.S., Smith, G.F., Chase, B.M., 2013. Quantification of climate change for the last 20,000 years from Wonderkrater, South Africa: implications for the long-term dynamics of the Intertropical Convergence Zone. Palaeogeography, Palaeoclimatology, Palaeoecology 386, 575-587.
Tyson, P.D., Cooper, G.R.J., McCarthy, T.S., 2002. Millennial to multi-decadal variability in the climate of southern Africa. International Journal of Climatology 22, 1105-1117.
van Aardt, A., Bousman, C.B., Brink, J.S., Brook, G.A., Jacobs, Z., du Preez, P.J., Rossouw, L., Scott, L., 2016. First chronological, palaeoenvironmental, and archaeological data from the Baden-Baden fossil spring complex in the western Free State, South Africa. Palaeoecology of Africa 33, 117-152.
van Zinderen Bakker, E.M., 1976. The evolution of late Quaternary paleoclimates of Southern Africa. Palaeoecology of Africa 9, 160-202.
Wang, B., Ding, Q., 2008. Global monsoon: dominant mode of annual variation in the tropics. Dynamics of Atmospheres and Oceans 44, 165-183.
Weldeab, S., Lea, D.W., Schneider, R.R., Andersen, N., 2007. 155,000 years of West African Monsoon and ocean thermal evolution. Science 316, 1303-1307.
Woodborne, S., Hall, G., Robertson, I., Patrut, A., Rouault, M., Loader, N.J., Hofmeyr, M., 2015. A 1000-year carbon isotope rainfall proxy record from South African baobab trees (*Adansonia digitata* L.). PLoS ONE 10, e0124202.
Yim, S.-Y., Wang, B., Liu, J., Wu, Z., 2014. A comparison of regional monsoon variability using monsoon indices. Climate Dynamics 43, 1423-1437.

Tables

Table 1: Radiocarbon ages and calibration information for the three adjoining sections of the Marakabi-1 rock hyrax midden.

Sample	Depth (mm)	^{14}C age yr BP	1 sigma error	calibration data	95.4 % (2σ) cal age ranges	95.4 % (2σ) cal age ranges	relative area under distribution	median probability (cal BP)
					lower cal range BP	upper cal range BP		
Section 1a								
UBA-23287	14.5929	F14C 1.1462	0.0028	SHZ1_2	-43.16	-40.65	92.7%	-42
					-9.65	-9.36	7.3%	
UBA-27044	41.8371	271	21	SHCal20	152	171	20.1%	289
					176	187	5.1%	
					194	211	6.7%	
					276	318	68.0%	
UBA-27045	77.5990	842	28	SHCal20	671	742	95.6%	707
					752	764	4.4%	
UBA-25779	100.9601	1765	21	SHCal20	1579	1701	100.0%	1651
UBA-25780	180.3128	2126	21	SHCal20	2000	2107	100.0%	2051
UBA-27046	211.6279	2204	27	SHCal20	2021	2024	0.3%	2141
					2056	2075	3.3%	
					2078	2155	52.8%	
					2169	2178	0.9%	
					2198	2204	0.4%	
					2226	2313	42.3%	
UBA-27047	241.1268	3127	25	SHCal20	3210	3378	100.0%	3293
UBA-25781	263.2353	3456	25	SHCal20	3574	3725	85.7%	3669
					3748	3769	3.9%	
					3793	3823	10.4%	
UBA-23288	332.1913	3552	26	SHCal20	3694	3887	100.0%	3782
Section 1b								
UBA-25775	-11.3984	1253	24	SHCal20	3833	3996	90.9%	3928
					4037	4080	9.1%	
UBA-27048	7.1560	3742	24	SHCal20	3927	3947	3.8%	4042
					3966	4151	96.2%	
UBA-25776	105.1927	4063	27	SHCal20	4414	4581	97.7%	4487
					4598	4614	1.7%	
					4772	4778	0.6%	
UBA-27049	118.1757	4058	27	SHCal20	4413	4580	99.1%	4484
					4601	4612	0.9%	
UBA-23289	200.5716	4426	36	SHCal20	4852	5054	90.0%	4960

					5110	5125	1.1%	
					5186	5268	8.8%	
UBA-27050	283.2230	4697	29	SHCal20	5312	5473	100.0%	5400
Section 1c								
UBA-27051	5.9	4519	25	SHCal20	4978	5009	5.9%	5161
					5032	5296	94.1%	
UBA-25777	54.9	4729	26	SHCal20	5319	5480	91.7%	5398
					5532	5571	8.3%	
UBA-27052	106.9	5393	32	SHCal20	6001	6089	33.5%	6139
					6104	6219	48.9%	
					6232	6278	17.6%	
UBA-25778	155.8	5536	28	SHCal20	6207	6242	16.0%	6298
					6270	6355	68.7%	
					6362	6394	15.4%	
UBA-23290	253.2	5907	29	SHCal20	6565	6584	3.0%	6696
					6609	6613	0.3%	
					6617	6787	96.7%	

Figures

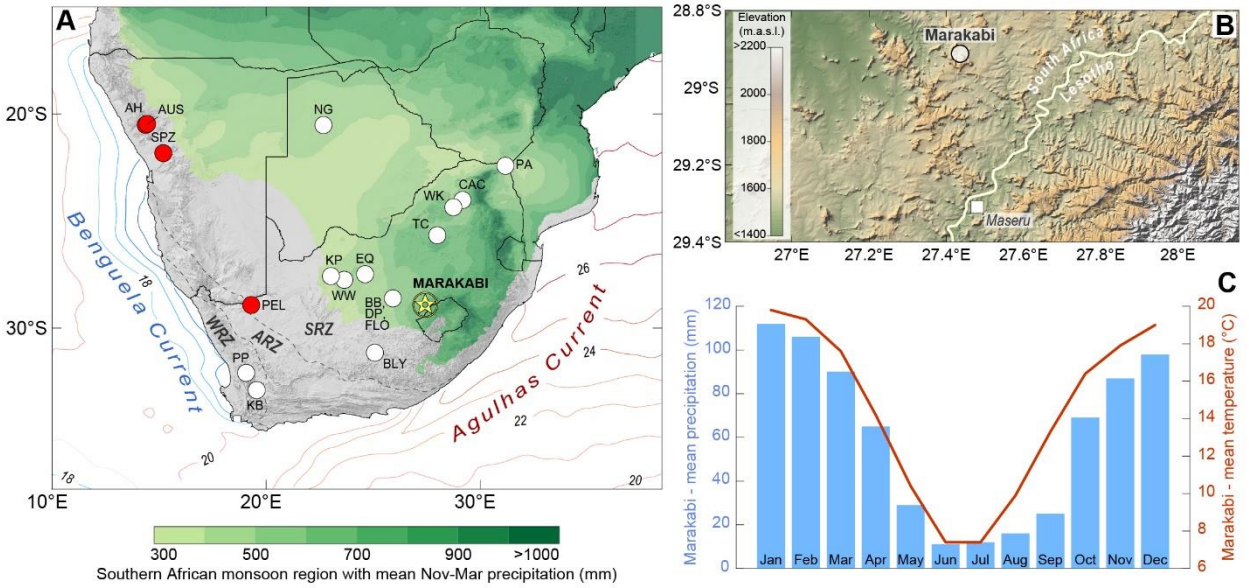

Figure 1: Regional and climatic context of the Marakabi rock hyrax midden site. **A**) Map of southern Africa with Marakabi site (yellow star) and the extent of the southern African monsoon region as defined by Wang and Ding (2008) indicated in green. Average summer sea-surface temperatures (NOAA/OAR/ESRL/PSL) and the position of the Benguela and Agulhas currents are shown, as the modern boundaries of the winter, summer and intermediate aseasonal rainfall zones (WRZ, ARZ, SRZ; sensu Chase and Meadows, 2007). The location of relevant Holocene palaeoenvironmental sites are indicated by white dots. Red dotes denote the Namib Desert rock hyrax middens. Sites are labelled as follows: Aba-Huab (AH; Chase et al., 2010), Austerlitz (AUS; Chase et al., 2010); Spitzkoppe (SPZ; Chase et al., 2009; Chase et al., 2019b), Pella (PEL; Chase et al., 2019b; Lim et al., 2016), Lake Ngami (NG; Burrough et al., 2007; Cordova et al., 2017), Pakhuis Pass (PP; Chase et al., 2019a; Scott and Woodborne, 2007a, b), Katbakkies Pass (KB; Chase et al., 2015b; Meadows et al., 2010), Blydefontein (BLY; Scott et al., 2005), Florisbad (FLO; Scott and Nyakale, 2002), Deelpan (DP; Scott, 1988), Baden-Baden (BB; van Aardt et al., 2016), Wonderwerk Cave (WW; Brook et al., 2010), Kathu Pan (KP; Beaumont et al., 1984; Scott, 1999; Sobol et al., 2022), Equus Cave (EQ; Scott, 1987), Tswaing Crater (TC; Metwally et al., 2014; Partridge et al., 1997; Scott, 1999), Wonderkrater (WK; Scott, 1982; Scott, 1999; Truc et al., 2013), Cold Air Cave (CAC; Holmgren et al., 2003; Lee-Thorp et al., 2001; Sundqvist et al., 2013), Pafuri (PA; Woodborne et al., 2015). **B**) Topographical relief map of the Marakabi region. **C**) Climograph for the Marakabi site (data from Fick and Hijmans, 2017).

Figure 2: Marakabi rock hyrax midden site: **A)** environment on plateau above midden site; **B)** Marakabi-1 midden prior to sampling (16 cm GPS unit for scale); **C)** view of midden site (under central overhang); **D)** Marakabi-1 midden after the section was taken from tallest central portion of midden.

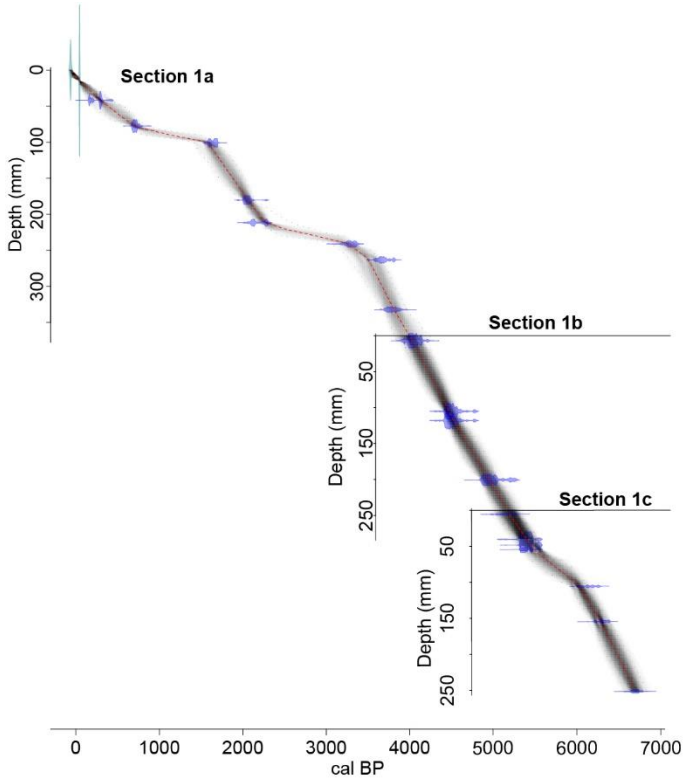

Figure 3: Age-depth models for the three adjoining sections of the Marakabi-1 rock hyrax midden.

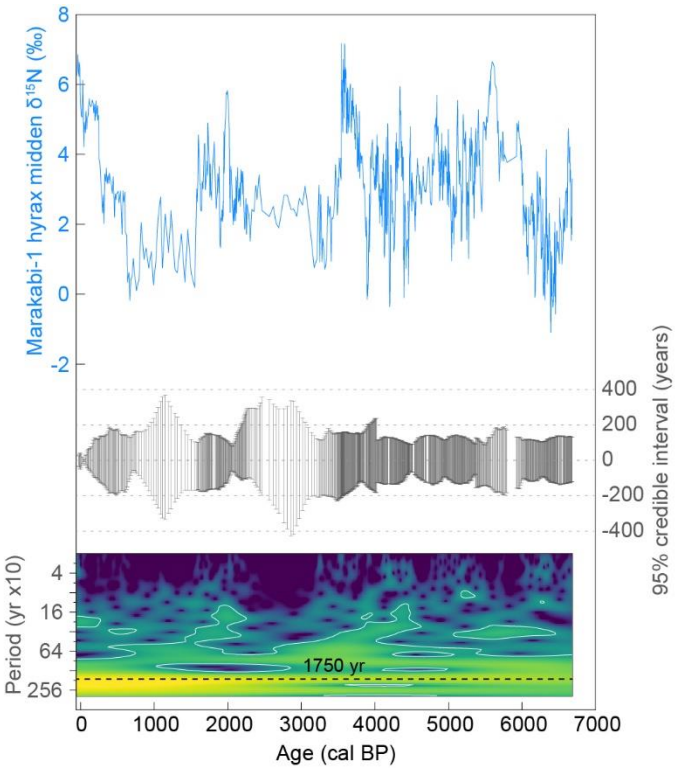

Figure 4: The $\delta^{15}N$ data from the Marakabi-1 rock hyrax midden. The data from the three adjoining sections have been compiled to create a single sequence. 95% credible intervals associated with the age-depth model for each sample are indicated. Lower pane shows local Morlet wavelet power spectrum for the $\delta^{15}N$ record, with white line delimiting greater than 95% confidence using a white-noise model (Hammer et al., 2001). Dominant ~1750-yr frequency is indicated by dashed line.

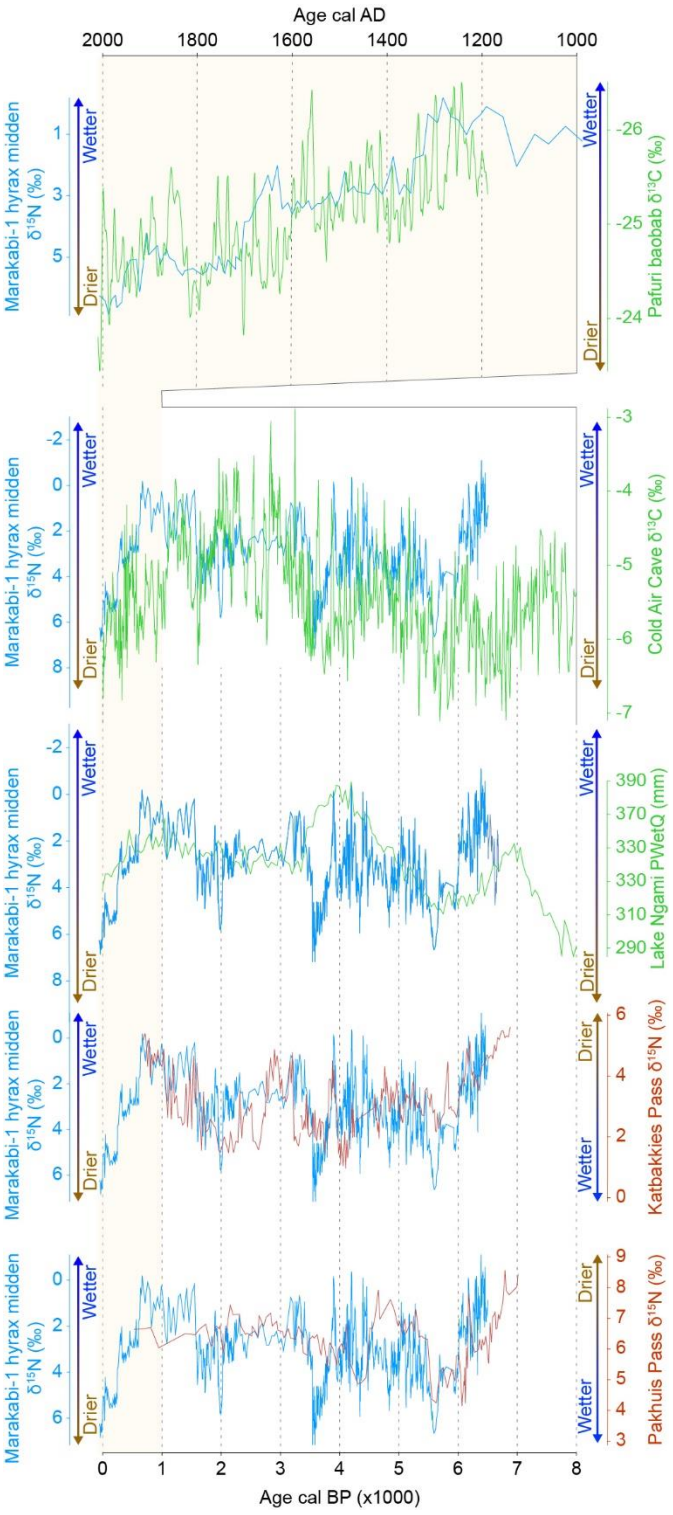

Figure 5: The $\delta^{15}N$ data from the Marakabi-1 rock hyrax midden compared with records from the southern African monsoon region (in green; the Pafuri baobabs (Woodborne et al., 2015) for last ~800 years (indicated by yellow shading), Lake Ngami (Cordova et al., 2017) and Cold Air Cave speleothems (Holmgren et al., 2003)) and the winter rainfall zone (in red; rock hyrax middens from Katbakkies Pass (Chase et al., 2015b) and Pakhuis Pass (Chase et al., 2019a)) that have been interpreted as indicators of humidity. Note that axes for the winter rainfall zone records have been inverted relative to the Marakabi-1 data to highlight the inverse nature of the relationship. See Figure 1 for site locations.

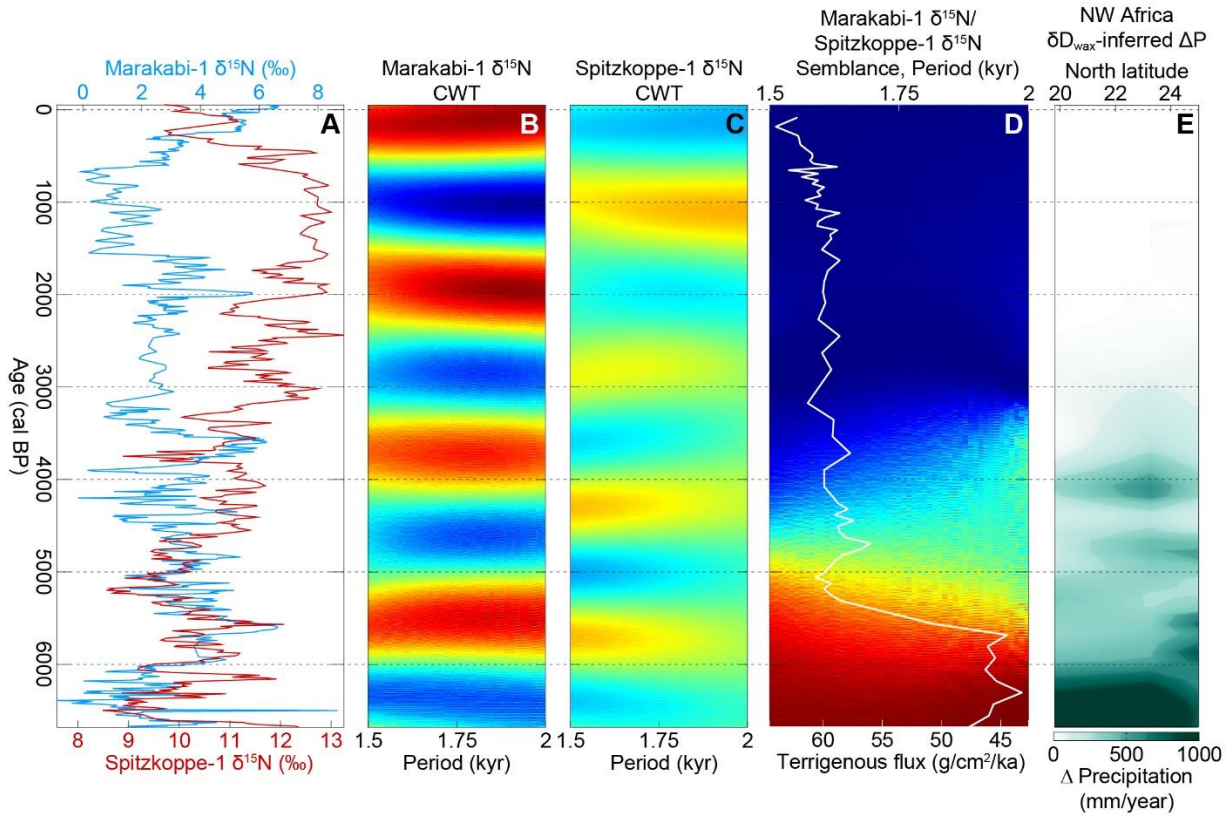

Figure 6: (**A**) The $\delta^{15}N$ data from the Marakabi-1 (this paper) and Spitzkoppe-1 (Chase et al., 2019b) rock hyrax middens. (**B, C**) Continuous Morlet wavelet transform (CWT) real-value signal power for the dominant 1750-yr frequency of these $\delta^{15}N$ records and (**D**) results of semblance analysis (Cooper and Cowan, 2008) of these records, wherein red indicates a semblance of +1 (positive correlation), and blue indicates a semblance of −1 (negative correlation). Also included in panel **D** is the Northwest African terrigenous dust flux record from marine core ODP 658C, which has been used to define an abrupt termination to the African Humid Period in the region (deMenocal et al., 2000). Panel **E** presents the dD_{wax}-inferred mean annual precipitation reconstructions of Tierney et al. (2017) from a suite of Northwest African marine cores (expressed as changes in precipitation relative to the 0-2500 cal BP mean). See Figure 1 for southern African site locations. (For interpretation of the references to colour in this figure legend, the reader is referred to the web version of this article.)

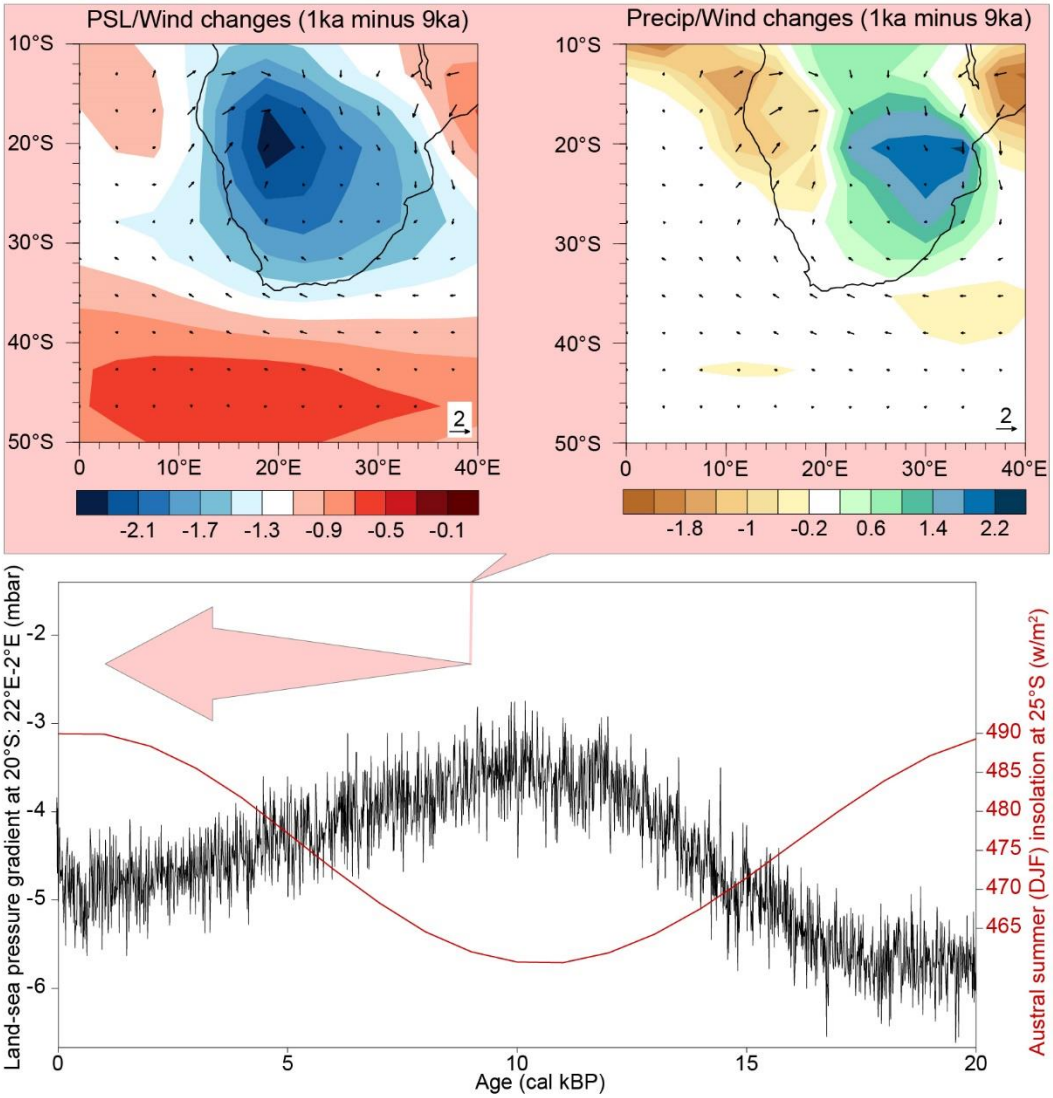

Figure 7: Orbital-scale dynamics determining phasing of southern African hydroclimates (after Chase et al., 2019b). TraCE21ka (Simulation of Transient Climate Evolution over the last 21,000 years; http://www.cgd.ucar.edu/ccr/TraCE/) simulations (He et al., 2013; Liu et al., 2009) of sea-level pressure (PSL), precipitation, and wind-field changes between late and early Holocene (1 ka minus 9 ka in red; arrow indicates direction of anomalies plotted in maps, from periods of lower (9 ka) to higher (1 ka) sea-level pressure). (For interpretation of the references to colour in this figure legend, the reader is referred to the web version of this article.)